

# Pulsatile gas-liquid flow resembling Decompression Sickness: Computational Fluid Dynamics simulation and experimental validation

Sotiris Evgenidis<sup>id</sup>, Thodoris Karapantsios<sup>id</sup>

Department of Chemical Technology and Industrial Chemistry, School of Chemistry, Aristotle University, Thessaloniki, Greece

## ABSTRACT

**Background:** This work performs two-dimensional Computational Fluid Dynamics (CFD) simulations of pulsatile bubbly flow in a column resembling the flow inside human vena cava during Decompression Sickness (DCS), aiming to illustrate the effect of certain parameters in bubbly blood flow and so facilitate the design of the: a) corresponding in-vitro bubbly flow experiments under pulsatile flow conditions inside a flow loop and b) in-vivo trials on swines for assessing a novel electrical impedance spectroscopy technique on the detection of bubbles (as those found during DCS) in their bloodstream.

**Materials and methods:** The commercially available ANSYS 2019-R3 CFD code was employed to simulate the pulsatile bubbly flow that resembled DCS. Simulations were validated against experiments conducted in a vertical co-current upward pulsatile bubbly flow provided by a flow loop equipped with electrical, optical and pressure diagnostics.

**Results:** CFD simulations under pulsatile conditions were initially validated by oscillatory in-vitro bubbly flow experiments. Then, the influence of pulsation parameters on void fraction,  $\alpha$ , and flow velocity,  $U$ , profiles was computationally investigated. Intense periodic fluctuations of void fraction were observed along the column and their intensity increases with pulsation amplitude. Moreover,  $U$  and  $\alpha$  radial profiles were uniform for bubbles 30  $\mu\text{m}$  but showed a core-peaking profile for bubbles 300  $\mu\text{m}$ .

**Conclusions:** CFD simulations of pulsatile bubbly flow resembling DCS provided unconventional information about the influence of different-sized sub-millimetre bubbles on the flow velocity and void fraction profiles, which are expected to improve the design of in-vitro and in-vivo trials for the detection of bubbles such as those found in DCS.

(Int Marit Health 2022; 73, 4: 189–198)

**Key words:** CFD, bubbly flow, Decompression Sickness, void fraction, flow velocity

## INTRODUCTION

Two-phase (gas-liquid) bubbly flow has been studied extensively for several decades, both theoretically and experimentally. The numerous applications of bubbly flow in different industries, however, makes researchers focus constantly on this, investigating in depth bubble dynamics and interactions, as well as the motion and phase distribution of two-phase systems that govern

principally the transfer processes. Bubbly flow is currently encountered in various engineering systems of chemical, petroleum, nuclear and food industries, such as heat exchangers, boilers, steam generators, phase separators, transport pipelines and chemical reactors [1]. All these applications take the advantage of high mixing properties and enhanced heat, mass and momentum transfer during bubbly flow [2].

✉ Dr. Sotiris P. Evgenidis, Department of Chemical Technology and Industrial Chemistry, School of Chemistry, Aristotle University, University Box 116, 541 24 Thessaloniki, Greece, tel/fax: +302310997798, e-mail: sevgenid@chem.auth.gr

Received: 23.11.2022 Accepted: 16.12.2022

This article is available in open access under Creative Common Attribution-Non-Commercial-No Derivatives 4.0 International (CC BY-NC-ND 4.0) license, allowing to download articles and share them with others as long as they credit the authors and the publisher, but without permission to change them in any way or use them commercially.

Most industrial applications concern steady bubbly flow. However, oscillatory bubbly flow is also found in some cases, increasing significantly the complexity of two-phase flow dynamic behaviour. The introduction of flow unsteadiness may be either beneficial or detrimental for the system under study. The pulsating heat pipes are novel heat transfer components with a simple structure and flexible arrangement, which are utilised in heat recovery systems, electronic cooling systems, space, automobiles, etc. The main difference between pulsating heat pipes and conventional heat pipes is the existence of reciprocating oscillatory flow that results in fast thermal response and higher heat transfer rate [3]. Sometimes, oscillatory bubbly flow can be also employed to enhance mass transfer in bubble columns [4]. On the other hand, the response of multiphase systems to periodic oscillations may be problematic. This is the case of bubbly flow observed in heat exchangers and power plants on-board ocean-going vessels. Unfavourable void fraction distribution in response to ocean waves may affect heat transfer, enhance thermal fatigue and even cause burnout in boiling systems [5].

Interestingly, oscillatory bubbly flow can be also found in human physiology when gas bubbles get into the blood stream during Decompression Sickness (DCS). DCS describes a condition where dissolved gases come out of solution into bubbles inside the human body, in response to acute reduction in ambient atmospheric pressure. It may be experienced in depressurisation events such as extra-vehicular activities of astronauts outside the spacecraft, working in a caisson, underwater diving decompression and flying in unpressurised aircraft [6, 7]. Furthermore, a few bubbles may accidentally enter the blood circulation and form a pulsating bubbly flow during cardio-vascular surgeries, due to extracorporeal blood circulation circuit malfunction. In both cases, bubbles presence may have mechanical, embolic, and biochemical effects with manifestations ranging from itching and minor pain to neurological symptoms, cardiac failure and death [8]. Although oscillatory bubbly flow during DCS is uninvited, it is helpful enough when resulting from purposeful introduction of bubbles in human bloodstream to block the blood supply to tumours in blood vessels [9].

In-depth understanding of two-phase flow behaviour (e.g. void fraction distribution and velocity profile) is necessary to enhance productivity and ensure safety in industrial applications, as well as to facilitate the prevention and treatment of DCS incidents in astronauts and divers. This can be achieved either experimentally or computationally. Experimental study of two-phase flow parameters is limited to lab scale and has to overcome possible technical constraints and high costs. On the other hand, computational modelling is simpler, less expensive and time-consuming and may be extended to larger scale [9]. Furthermore, recent advances

in Computational Fluid Dynamics (CFD) multiphase flow domain allow investigating pretty complicated problems much more thoroughly and accurately than simplified models and experimental methods can do. Ideally, modelling is performed complementary to experimental work, but even individually provides valuable information on multiphase flow physics.

Most CFD studies focus on turbulent bubbly flow because of its numerous applications in industry. Laminar bubbly flow, however, is a significant limiting case, whose dynamics are not yet understood completely (“laminar” and “turbulent” flow refers to liquid single-phase flow). Actually, flows generated by injecting bubbles into laminar bulk flow exhibit a “pseudo-turbulent” behaviour that is interesting to investigate [10]. Previous studies have shown that the distribution of void fraction, the key parameter to describe the inter-phase interactions in bubbly flow, varies considerably with the flow conditions and depends strongly on bubble size (referring to uniform bubble size in the order of magnitude of a few mm). For bubbles smaller than 2 mm (nearly spherical bubbles) in upward flows, void fraction distribution is relatively uniform in the core of the channel and has a peak near the pipe walls. For bubbles greater than 3.5–4.0 mm (sufficiently deformable bubbles), on the other hand, void fraction distribution peak shifts to the pipe centre [10, 11]. Interestingly, two-peak void fraction distribution has been also found in laminar bubbly flow for varying experimental conditions, e.g. with bubbles around 2.3 mm and average void fraction of 0.01–0.02 in a pipe of 14.8 mm inner diameter [12]. Void fraction distribution becomes more complex for non-uniform bubble sizes, since distinct bubble sizes have different distributions in the same bubbly flow. The different phase distributions for the small and large bubbles create a more intense fluctuating flow field that flattens void fraction profile peaks [11].

Although literature lacks of CFD studies for bubbly flow in human physiology, several authors have performed computational modelling to solve and analyse problems including blood flow. The majority of these studies investigated blood flow parameters under pathological conditions related to atherosclerosis and cardiovascular diseases. CFD is an appropriate tool to estimate such quantities, since it produces results in fair agreement with those obtained from in-vivo tests that need expensive and specialized medical devices [13, 14].

This work is complementary to previous studies that investigated experimentally the case of vertical, co-current, upward, steady gas-liquid flow, where the examined conditions resemble bubbly flow in human vena cava during DCS [15–19]. Despite the different local characteristics, similar average bubbly flow conditions, combining sub-mil-

limetre bubbles and low void fractions ( $< 10^{-1}$ ), are also encountered in other two-phase flow applications, e.g. flow boiling in macro-channels [20]. Void fraction and bubble size distribution were studied in a fully automated flow loop employing electrical resistance tomography, an European Union patented ultra-sensitive electrical impedance spectroscopy technique (called I-VED) [21], as well as optical and pressure diagnostics. In addition, measured void fraction values were compared against predicted ones employing well-known drift-flux model based correlations [22]. Here, two-dimensional (2D) CFD simulations were carried out to investigate for the first time axial and radial void fraction distribution as well as velocity profile in this kind of bubbly flow under both steady and pulsatile flow conditions. The primary objective of the study was to facilitate the design of the forthcoming: a) in-vitro experiments for the investigation of bubbly flow resembling DCS under pulsatile flow conditions and b) in-vivo trials on swines for assessing the performance of the abovementioned I-VED electrical impedance method on the detection of infused bubbles (as those found during DCS) in their bloodstream. Validity of CFD simulations in such conditions was assessed with respect to preliminary in-vitro experimental results. Furthermore, this work aimed to compare CFD simulations with the experimental and drift-flux model findings for steady flow conditions and to extend knowledge obtained from experimental studies providing detailed information on the spatial and temporal distribution of the two phases and local bubbly flow peculiarities.

## MATERIALS AND METHODS

### PROBLEM FORMULATION

The vertical co-current upward bubbly flow that resembles DCS conditions was simulated employing the commercially available ANSYS 2019 R3 CFD code. The vertical column flow problem was simplified down to a 2D axisymmetric case. The height,  $h$ , and the inner diameter of the column,  $D$ , were 1000 mm and 21 mm (equal to the diameter of human vena cava where bubbles gather during a decompression incident), respectively [8]. Thus, a computational grid was developed consisting of 21,000 elements ( $1000 \times 21$ ) sized from 0.2 to 1 mm, since they are biased near the wall to capture adequately the laminar boundary layer.

Bubbly flow inside the vertical column was modelled by means of the Eulerian multiphase model. Although the most complex one, it is considered tractable enough for this kind of two-phase flow by averaging the equations in space. The two phases are assumed as interpenetrating and interacting continua and separate momentum and mass balance equations are solved for each phase. An advantage of this approach is the convenient two-way coupling between phases [23].

**Table 1.** Liquid-gas properties at 37 °C and parameters used for two-dimensional simulations (varying parameters in blue colour)

Liquid density [kg/m <sup>3</sup> ]	1050	
Liquid viscosity [mPa.s]	4.5	
Mean liquid velocity, $U_{l,mean}$ [cm/s]	3	30
Sinusoidal pulsation frequency [Hz]	1	
Sinusoidal pulsation amplitude [% of $U_{l,mean}$ ]	10	50
Gas density [kg/m <sup>3</sup> ]	1.225	
Gas viscosity [mPa.s]	$1.79 \times 10^{-2}$	
Bubble diameter, $D_b$ [ $\mu$ m]	30	300
Void fraction, $\alpha$ [-]	0.03	0.10
Gravitational acceleration [m/s <sup>2</sup> ]	9.81	

Liquid and gas properties as well as parameters used for 2D simulations are listed in Table 1. All physical properties were taken at 37°C, equal to body temperature. Liquid density and viscosity (supposing Newtonian behaviour) simulate blood physical properties, while the applied mean liquid velocities,  $U_{l,mean} = 3$  and 30 cm/s, are representative of blood-stream in human vena cava [8, 24]. For the abovementioned liquid flow rates, the Reynolds number of single liquid phase is 147 and 1470, respectively. Therefore, a laminar flow profile was used as a boundary condition. Pulsating liquid flow was simplified to a sinusoidal flow profile of 1 Hz (corresponding to 60 heart beats) with varying amplitude ( $\pm 10\%$  and  $\pm 50\%$  of average flow rate). To compare with, steady bubbly flow simulations were also performed. Gas physical properties correspond to air for simplicity. Two low void fraction values,  $\alpha = 0.03$  and 0.10, as well as two sub-millimetre bubble diameters,  $D_b = 30$  and 300  $\mu$ m, were also tested in the simulations. To clearly investigate the effect of bubble size on the examined parameters, monodisperse bubble size distributions were only studied. Thus, no mixed bubble size case was tested. A gravity term was also included to account for the buoyancy of the bubbles. The results of 2D simulations are presented in several plots shown below, demonstrating the effect of varying parameters listed in Table 1 on the axial and radial distribution of void fraction and velocity.

### EXPERIMENTAL SETUP

Experimental setup for steady flow conditions and applied diagnostics have been previously described in details and, thus, a concise description is given below [15, 16, 18, 19]. Measurements were conducted in a vertical co-current upward bubbly flow provided by a fully controllable

flow loop. The main part of the loop consisted of a vertical tube with inner diameter  $D = 21$  mm (equal to that used in simulations) that accommodates successive test sections of electrical, optical, acoustical and pressure diagnostics employed for void fraction, bubble size and bubble velocity measurements. Test liquid was recirculated by means of a progressive cavity pump (MD 025-6L, Motovario S.p.A.) and bubbles were injected through a cylindrical glass microporous filter (ROBU<sup>®</sup>; nominal pore size: 1.0–1.6  $\mu\text{m}$ ) located at the bottom of the vertical tube. Pulsatile flow conditions were generated by an intermittent flow module consisting of a proportional electromagnetic valve (PSV, electromagnetic valve, Alborg) driven through a signal produced by a function generator (20 MHz Function/Arbitrary Waveform Generator, 33220A, Agilent) and modulated by an electronic driver (PSV-D Driver Module, Alborg). Proper tuning of signal features enables application of varying pulsation frequencies, amplitudes and profiles (sinusoidal, triangular or rectangular). To facilitate validation of CFD simulations, a sinusoidal flow profile with a frequency of 1 Hz and amplitude of  $\pm 50\%$  was applied in this study.

Void fraction measurements were performed by means of an European Union patented, highly accurate and sensitive electrical impedance spectroscopy technique that allows capturing void fraction fluctuations down to  $10^{-5}$  [21]. The operation of this technique has been previously described analytically by the authors [15]. Electrical measurements were conducted by a pair of ring electrodes (electrode width:  $D/10$ , separation distance:  $D/4$ ) located at an axial distance of 59 cm ( $\sim 28 D$ ) above the gas injection point and synchronised with bubble size measurements applying an optical method described by the authors in previous studies [15, 16]. Bubble size determination was based on image processing of bubbly flow images captured at three radial positions inside the vertical tube ( $r = 0$ ,  $r = D/4$  and  $r = D/2$ ) at an axial distance of 75 cm ( $\sim 36 D$ ) above the gas injection point.

For the needs of the preliminary tests under pulsatile flow conditions, an aqueous solution of NaCl 0.02% w/w (purity  $> 99.5\%$ , Merck KGaA) resembling the electrical conductivity of tap water was used as test liquid. Bubbles were produced by Helium gas (purity 99.9996%, Air Liquide) due to its low solubility in the liquid phase. In order to limit substantially bubble size polydispersity, 500 ppm of the surface active agent sodium dodecyl sulphate (SDS, purity  $> 99.0\%$ , Fluka Biochemika) was added in the test liquid resulting in bubbles around 100  $\mu\text{m}$ . Liquid temperature was adjusted at the body temperature, 37°C. Measured physical properties of the test liquid at 37°C were: i) surface tension: 37.0 mN/m, ii) density: 991  $\text{kg}/\text{m}^3$ , iii) electrical conductivity: 0.5 mS/cm, and iv) dynamic viscosity: 0.70 mPa.s. Measurements were conducted for liquid superficial velocity,  $U_{sl} = U_{l,mean} = 3$  cm/s (Reynolds number of liquid phase equal to 860, laminar flow)

and gas superficial velocity  $U_{sg} = 0.217$  cm/s, that provides void fraction values at the same order of magnitude with those calculated from CFD simulations and, in parallel, clear pulsatile void fraction fluctuations.

## RESULTS

### VALIDATION OF CFD SIMULATION WITH EXPERIMENTAL RESULTS

Here, calculated void fraction is compared against measured one for vertical, co-current, upward bubbly flow, when employing a sinusoidal flow profile with a frequency of 1 Hz and amplitude of  $\pm 50\%$  for  $U_{l,mean} = 3$  cm/s. Figure 1 presents the evolution of calculated centreline void fraction,  $\alpha_c$ , and centreline flow velocity,  $U_c$ , as a function of column height, when the set parameters at the pipe inlet are:  $\alpha = 0.03$ ,  $U_{l,mean} = 3$  cm/s, pulsation amplitude:  $\pm 50\%$  and  $D_b = 300$   $\mu\text{m}$ . Numbering of void fraction pulsations has been added for convenience in Figure 1A. As shown, 8 full pulsations occur for  $U_{l,mean} = 3$  cm/s along the column height of 1 m. Contrary to CFD simulations that provide axial distribution of void fraction along the column height, experimental study of bubbly flow provides time-series of void fraction signals at a specific column height (59 cm). To facilitate the comparison, height values of x axis (Fig. 1A) were converted to time values when divided by  $U_c = 12$  cm/s, that corresponds to  $h = 590$  mm as shown in Figure 1B. As a result, Figure 1A is transformed to a time-series of calculated centreline void fraction at 59 cm. Although measured void fraction concerns the entire cross-section of the column, it is still interesting to compare the features of experimental  $\alpha$  and calculated  $\alpha_c$  time-series at the same column height (59 cm) and flow conditions ( $U_{l,mean} = 3$  cm/s and sinusoidal flow profile with a frequency of 1 Hz and amplitude of  $\pm 50\%$ ), Figure 2A. Despite the differences in average void fraction values, bubble sizes and liquid properties, periodic signal fluctuations due to pulsatile flow were clearly shown in both cases. Although duration and amplitude of observed pulsations in the experimental time-series did not vary considerably, they were both attenuating as a function of time in the signal resulted from CFD simulation. Figures 2B, C present the duration and the coefficient of variation (CV) of centreline void fraction (standard deviation of  $\alpha_c$ /average value of  $\alpha_c$ , %), respectively, for each one of the eight pulsations found in  $\alpha_c$  time-series of Figure 2A. To compare with, experimental average values of duration and CV of  $\alpha$  are also displayed in Figures 2B, C. It was demonstrated that both experimental average values are between those referring to 4<sup>th</sup> and 5<sup>th</sup> pulsation of calculated signal. Based on Figure 1A, this corresponds to a column height of  $\sim 60$  cm that coincides with the height where measurements were taken. Therefore, the validity of CFD simulations was confirmed by the experimental measurements and the influence

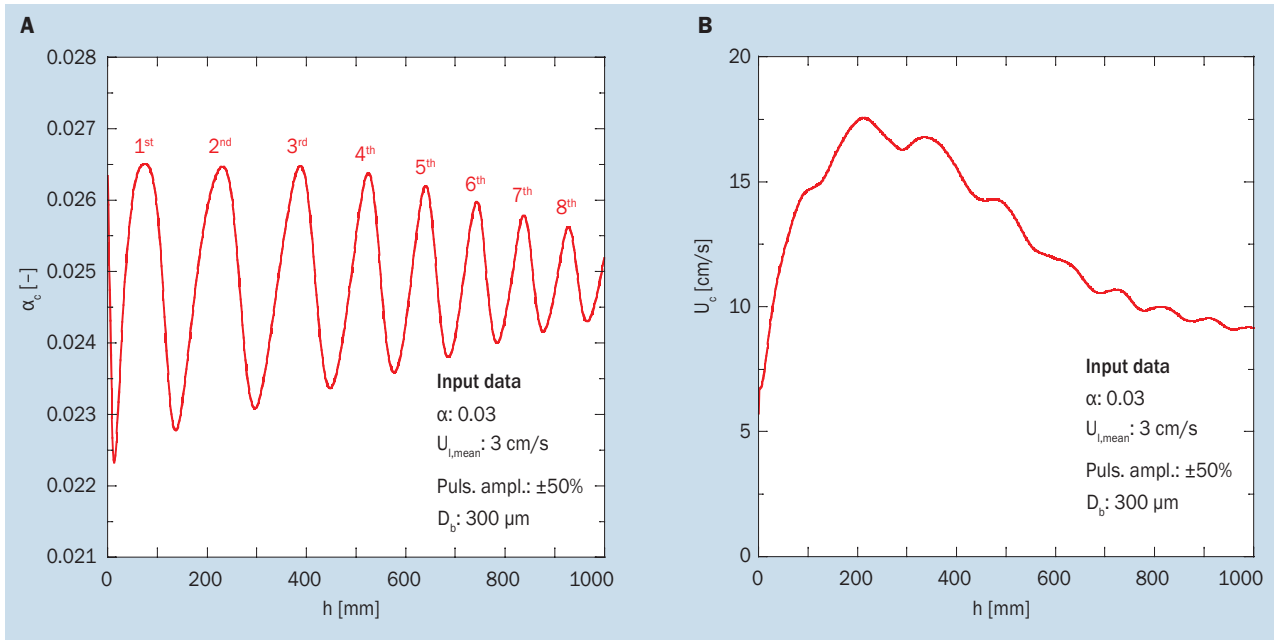


**Figure 1.** Axial distribution of calculated centreline void fraction,  $\alpha_c$  (A) and calculated centreline flow velocity,  $U_c$  (B), along the column for pulsatile (sinusoidal) flow. Input data:  $\alpha = 0.03$ ,  $U_{l,mean} = 3$  cm/s, pulsation frequency: 1 Hz, pulsation amplitude:  $\pm 50\%$ ,  $D_b = 300 \mu\text{m}$

of several parameters on void fraction and velocity profiles was next studied in depth computationally.

### EFFECT OF VARYING PARAMETERS ON VOID FRACTION AND FLOW VELOCITY PROFILES

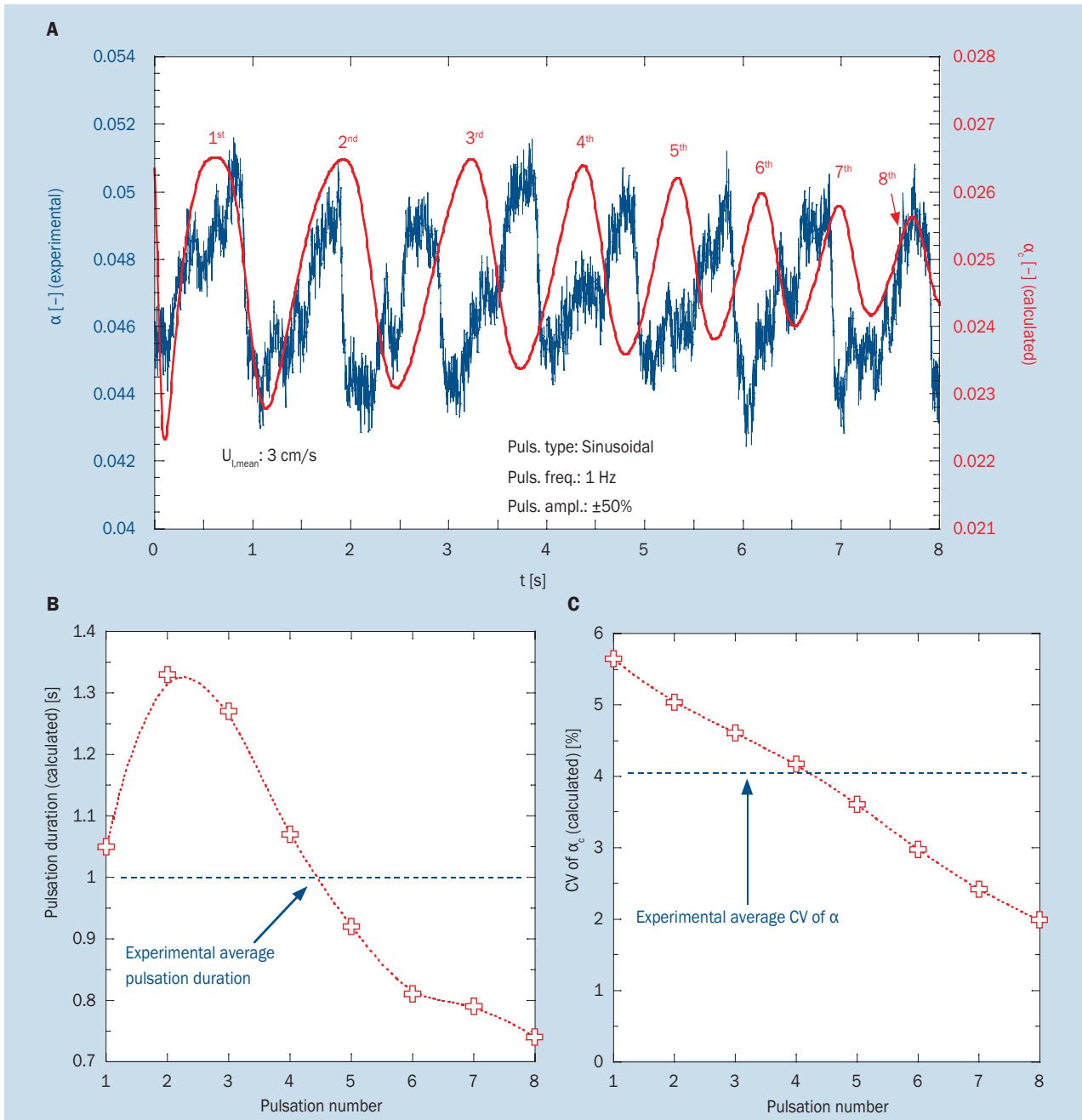
Figure 3 shows the effect of bubble size,  $D_b$ , on the flow velocity,  $U$ , and void fraction,  $\alpha$ , contour plots for pulsatile (sinusoidal) flow conditions. Two monodisperse bubble size distributions of  $30 \mu\text{m}$  and  $300 \mu\text{m}$  were examined, while the set parameters at the inlet of the vertical column were:  $\alpha = 0.10$ ,  $U_{l,mean} = 3$  cm/s, pulsation frequency: 1 Hz, pulsation amplitude:  $\pm 50\%$ . For  $D_b = 30 \mu\text{m}$ , both flow velocity and void fraction radial profiles were pretty uniform. For  $D_b = 300 \mu\text{m}$ , on the other hand, flow velocity and void fraction presented a core-peaking profile. In addition, an oscillating fluctuation of both quantities was clearly noticed along the column, which attenuated with the increase in axial distance from the entrance of the column. Hereafter, simulations were performed with  $D_b = 300 \mu\text{m}$  according to the obtained results.

Figure 4 examines the effect of pulsation amplitude on the axial distribution of centreline void fraction,  $\alpha_c$ , for two  $\alpha$  values, 0.03 and 0.10, and  $U_{l,mean} = 3$  cm/s at the inlet of the column. Centreline void fraction was always lower than the set values (Fig. 4A, B) since bubbles accelerated significantly due to buoyancy resulting in the depletion of the column from bubbles. For steady flow,  $\alpha_c$  was almost constant along the column. This agrees with previous experimental findings of the authors who investigated the axial evolution of void fraction in similar conditions by means

of electrical resistance tomography and differential pressure sensors, without observing any significant variation [16]. When employing pulsatile flow conditions, intense periodic fluctuations of  $\alpha_c$  could be noticed, while the mean void fraction was marginally reduced only for the pulsation amplitude of  $\pm 50\%$  ( $\sim 2\%$ ). These fluctuations verged on a sinusoidal form, in accordance to the input liquid flow profile, and their intensity increased with pulsation amplitude and set void fraction value. On the contrary, the amount of  $\alpha_c$  fluctuations for the column height of 1 m decreased when increasing  $\alpha$  value at the inlet of the column. Also, it is interesting to notice that  $\alpha_c$  pulsation amplitude depreciated progressively along the column for the lower input  $\alpha$  value, while this behaviour was not observed for the higher input  $\alpha$  value.

Next, the radial distribution of flow velocity,  $U$ , and void fraction,  $\alpha$ , was studied for sinusoidal flow of blood simulant with pulsation amplitude of  $\pm 50\%$  in the presence of bubbles with  $D_b = 300 \mu\text{m}$ . Figure 5 shows the evolution of  $U$  and  $\alpha$  as a function of column radius,  $R$ , with input data  $\alpha = 0.10/U_{l,mean} = 3$  cm/s and  $\alpha = 0.03/U_{l,mean} = 30$  cm/s. All radial distributions are given for 4 axial positions along the column:  $y = 0$  mm (pipe inlet),  $y = 250$  mm,  $y = 500$  mm,  $y = 750$  mm ( $y$ : axial distance from the entrance of the column). Apart from the core-peaking profile of  $U$  and  $\alpha$ , already observed in Figure 3, which is depicted more clearly in Figure 5, some more comments can be also made:

- For  $U_{l,mean} = 3$  cm/s ( $Re = 147$ ) and  $\alpha = 0.10$ ,  $U$  increased considerably for  $R = 0$  mm (pipe centre), due



**Figure 2.** A. Comparison of experimental cross-sectional averaged void fraction,  $\alpha$ , and calculated centreline void fraction,  $\alpha_c$ , time-series at the same column height (59 cm) and flow conditions ( $U_{l,mean} = 3$  cm/s and sinusoidal flow profile with a frequency of 1 Hz and amplitude of  $\pm 50\%$ ); Duration (B) and coefficient of variation (CV) (C) of centreline void fraction for each one of the eight pulses found in  $\alpha_c$  time-series of Figure 1 (experimental average values of duration and CV of  $\alpha$  are also denoted for comparison)

to the acceleration of bubbles, at  $y = 250$  mm. This increase attenuated radially up to  $R = 5$  mm and, then,  $U$  decreased in comparison to  $y = 0$  mm. Finally, it became zero at the pipe wall ( $R = 10.5$  mm), as shown in Figure 5A. Interestingly, limited reverse flow could be noticed near the pipe wall (slightly negative  $U$  values). The opposite trend, as expected, was observed for the radial profile of void fraction (Fig. 5B). At  $y = 250$  mm,

$\alpha$  decreases from  $R = 0$  mm to  $R = 5$  mm when compared to  $y = 0$  mm. This decrease was minimum at the pipe centre and increased radially up to  $R = 5$  mm. Next, void fraction slightly recovered because of the reverse flow near the pipe wall, but still remained lower than that at  $y = 0$  mm. Finally,  $\alpha$  got zero value at  $R = 10.5$  mm. At higher axial positions inside the column,  $U$  and  $\alpha$  radial profiles did not vary substantially any more.

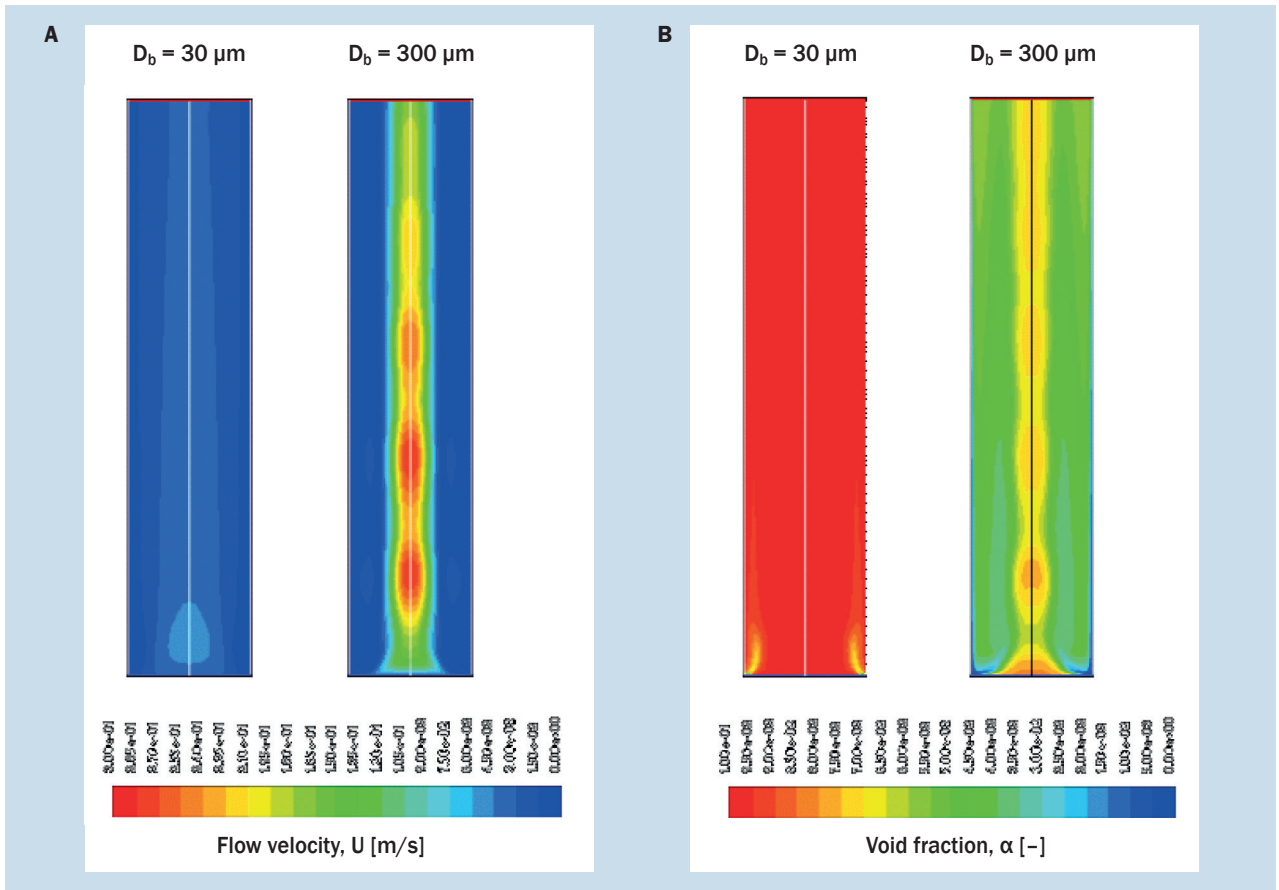


**Figure 3.** Effect of bubble size,  $D_b$ , on the flow velocity,  $U$ , (A) and void fraction,  $\alpha$ , (B) contour plots for pulsatile (sinusoidal) flow with input data:  $\alpha = 0.10$ ,  $U_{l,mean} = 3$  cm/s, pulsation frequency: 1 Hz, pulsation amplitude:  $\pm 50\%$ . The height dimension has been compressed by a factor of 10

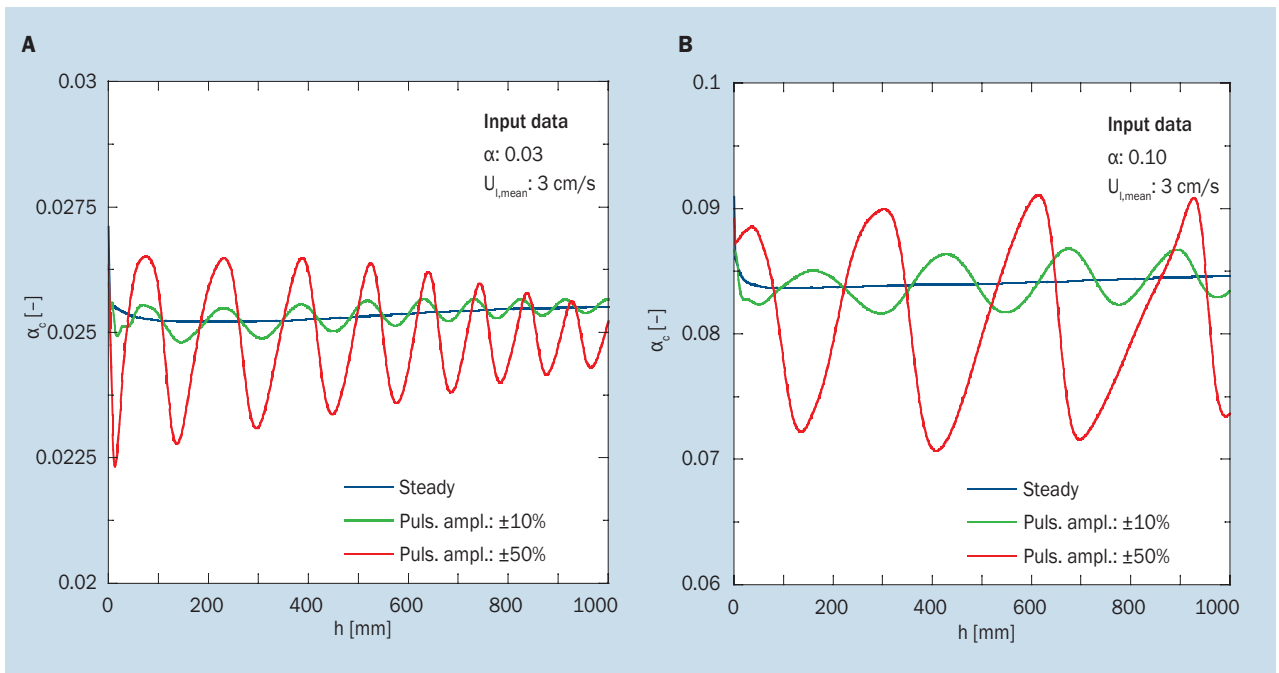


**Figure 4.** Axial distribution of centreline void fraction,  $\alpha_c$ , along the column for steady and pulsatile (sinusoidal) flow at different pulsation amplitudes. Input data:  $\alpha = 0.03$  (A);  $\alpha = 0.10$  (B);  $U_{l,mean} = 3$  cm/s, pulsation frequency: 1 Hz,  $D_b = 300 \mu\text{m}$

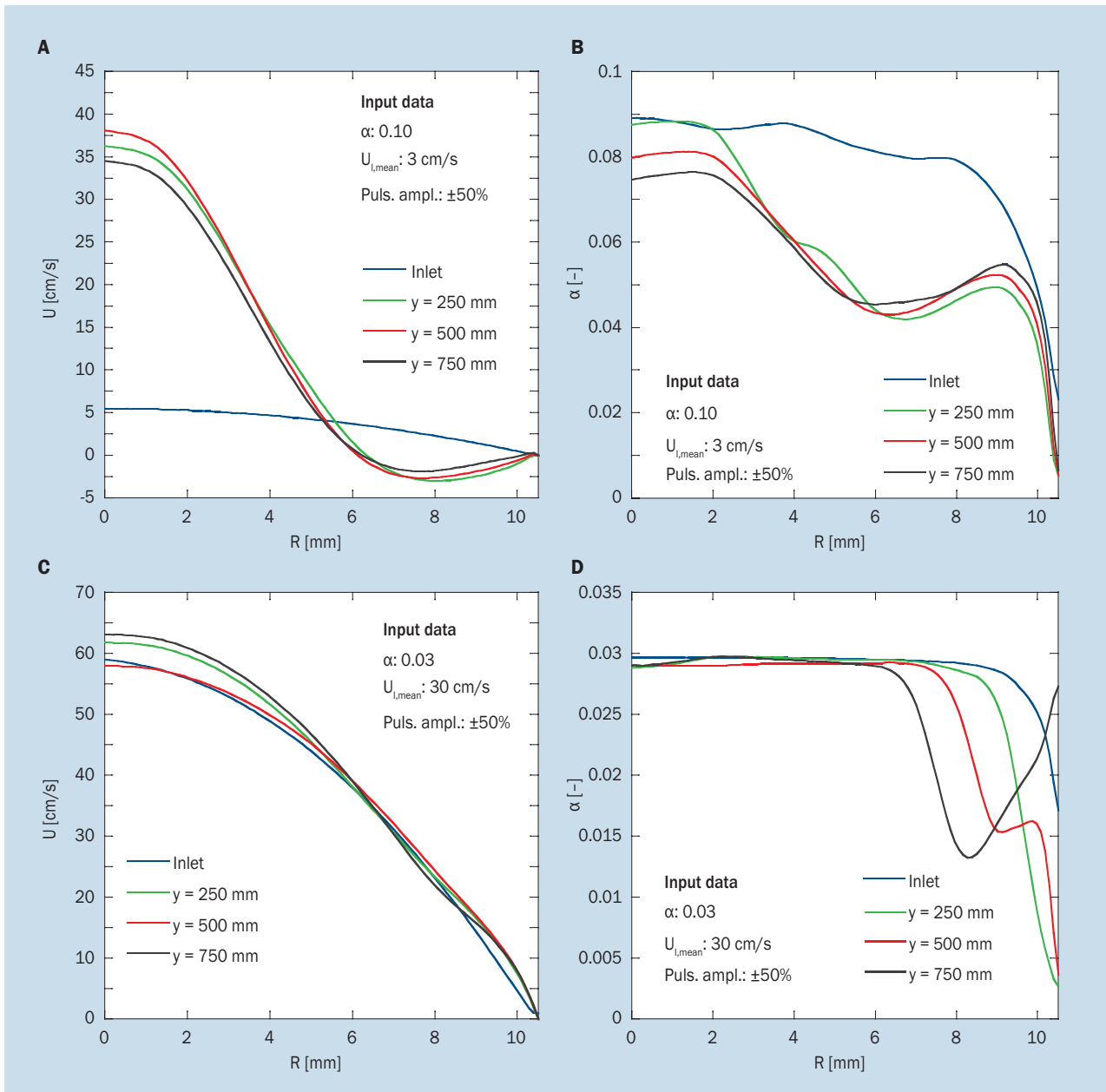


**Figure 5.** Radial distribution of flow velocity,  $U$  (A), and void fraction,  $\alpha$  (B), with input data:  $\alpha = 0.10$ ,  $U_{l,mean} = 3$  cm/s, pulsation frequency: 1 Hz, pulsation amplitude:  $\pm 50\%$ ,  $D_b = 300$   $\mu$ m and flow velocity,  $U$  (C), and void fraction,  $\alpha$  (D), with input data:  $\alpha = 0.03$ ,  $U_{l,mean} = 30$  cm/s, pulsation frequency: 1 Hz, pulsation amplitude:  $\pm 50\%$ ,  $D_b = 300$   $\mu$ m, at different axial positions along the column for pulsatile (sinusoidal) flow

b) For  $U_{l,mean} = 30$  cm/s ( $Re = 1470$ ) and  $\alpha = 0.03$ , Figure 5C shows that  $U$  radial profile remains almost constant along the column. Referring to the radial distribution of void fraction (Fig. 5D), the core-peaking profile is less sharp comparing to Figure 5B, while  $\alpha$  decreases near the pipe wall at higher axial positions inside the column.

## DISCUSSION

Aiming to facilitate the design of a) in-vitro pulsatile bubbly flow experiments in a column resembling the flow in-

side human vena cava during DCS in astronauts and divers and b) in-vivo trials on swines for assessing the performance of I-VED technology on the detection of infused bubbles (as those found during DCS) in their bloodstream [21], a number of CFD simulations was performed to investigate both steady and oscillatory gas-liquid flow of sub-millimetre bubbles at low void fractions ( $< 0.10$ ). Similar bubbly flow conditions were encountered in other two-phase flow applications, e.g. flow boiling in macro-channels, as well [20]. Validity of simulations was first confirmed by preliminary in-vitro bubbly flow



experiments under pulsatile flow conditions inside a fully controllable flow loop, when comparing observed pulsation characteristics: at the same column height, average duration and amplitude of pulsations captured in the experimental void fraction signals coincided with those of the calculated signals.

Next, the influence of varying parameters on void fraction and flow velocity profiles was computationally investigated. Comparing two monodisperse bubble size distributions with  $D_b = 30$  and  $300 \mu\text{m}$ , it was demonstrated that flow velocity and void fraction radial profiles are uniform for the small bubbles and present a core-peaking profile for the large ones. Since void fraction core-peaking profile is characteristic for bubbles greater than  $4 \text{ mm}$  [10, 11], it is interesting to notice this behaviour for much smaller ones ( $300 \mu\text{m}$ ) under such special conditions. Although  $\alpha$  and  $U_{l,\text{mean}}$  at the inlet of the column were equal for the two distinct  $D_b$  values, void fraction was much lower and flow velocity was much higher for  $D_b = 300 \mu\text{m}$ . This was due to the effect of buoyancy that accelerates only the large bubbles in comparison with the liquid velocity. Therefore, these bubbles rised with higher velocity and their residence time in the column decreased, resulting in lower void fraction [10]. The abovementioned results are in fair agreement with previous experimental and drift-flux model findings of the authors for steady flow conditions. Specifically, the dependence of void fraction on bubble size has been validated by performing experiments with Newtonian and non-Newtonian blood simulant test liquids at  $U_{l,\text{mean}} = 3\text{--}30 \text{ cm/s}$  and  $\alpha = 0.001\text{--}0.1$ , for two average diameters of polydisperse bubble size distributions which are comparable to the two  $D_b$  values used in the simulations [16, 19]. Furthermore, the authors examined the performance of thirteen drift-flux model based correlations on the prediction of void fraction under the abovementioned experimental conditions and concluded that: a) in the case of small bubbles, homogeneous flow model predicts accurately void fraction. This model is a sub-case of drift-flux model, implying uniform void fraction profile across the pipe and zero drift velocity of rising bubbles (they travel with liquid velocity), and b) in the case of large bubbles, three drift-flux models, suggesting core-peaking void fraction conditions, succeed to correlate adequately experimental data, applying King (2001) [25] model for drift velocity calculation [22].

Pulsatile flow conditions caused intense periodic fluctuations of void fraction along the column, whose intensity increased with pulsation amplitude and void fraction. Also, the amount of  $\alpha_c$  fluctuations for the column height of  $1 \text{ m}$  decreased when increasing  $\alpha$  value at the inlet of the column. This was attributed to the increased flow velocity for denser bubbly flows where more bubbles accelerate due to buoyancy. Specifically, the maximum centreline flow velocity for  $\alpha = 0.10$  was approximately double the velocity for  $\alpha = 0.03$  ( $\sim 35 \text{ cm/s}$  vs.  $\sim 18 \text{ cm/s}$ ). Inversely,


the amount of  $\alpha_c$  pulsations for  $\alpha = 0.10$  was half of that for  $\alpha = 0.03$  (4 pulsations vs. 8 pulsations).

The radial distribution of flow velocity for  $D_b = 300 \mu\text{m}$  evolved considerably along the column with the decrease in liquid velocity and the increase in void fraction. This behaviour was attributed to the enhancement of bubbles' drift velocity contribution as bubbly flow becomes denser and liquid flow slower [22, 25]. Void fraction profile varied axially accordingly.

## CONCLUSIONS

In conclusion, CFD simulations of pulsatile bubbly flow resembling DCS conditions, which were validated by in-vitro pulsatile bubbly flow experiments, provided unconventional information about the influence of different-sized sub-millimetre bubbles on the flow velocity and void fraction profiles. Observed core-peaking void fraction conditions will be seriously taken into consideration when designing electrodes configuration (e.g. geometry and distance of electrodes that affect the sensitivity and the measuring volume inside the vessel under study) of I-VED electrical impedance spectroscopy technique for bubbles detection both in-vitro in a flow loop and in-vivo in the bloodstream of swines.

## ACKNOWLEDGEMENTS

This study was funded by  ESA GSTP Project: In-Vivo Embolic Detector, I-VED – Contract No: 4000101764. The view expressed herein can in no way be taken to reflect the official opinion of the European Space Agency.

**Conflict of interest:** None declared

## REFERENCES

1. Peña-Monferrer C, Monrós-Andreu G, Chiva S, et al. A CFD-DEM solver to model bubbly flow. Part II: Critical validation in upward vertical pipes including axial evolution. *Chem Eng Sci.* 2018; 177: 537–556, doi: [10.1016/j.ces.2017.11.032](https://doi.org/10.1016/j.ces.2017.11.032).
2. Liao Y, Upadhyay K, Schlegel F. Eulerian-Eulerian two-fluid model for laminar bubbly pipe flows: Validation of the baseline model. *Comput Fluids.* 2020; 202: 104496, doi: [10.1016/j.compfluid.2020.104496](https://doi.org/10.1016/j.compfluid.2020.104496).
3. Sun X, Li S, Jiao Bo, et al. Experimental study on hydrogen pulsating heat pipes under different number of turns. *Cryogenics.* 2020; 111: 103174, doi: [10.1016/j.cryogenics.2020.103174](https://doi.org/10.1016/j.cryogenics.2020.103174).
4. Roig V, Roudet M, Risso F, et al. Dynamics of a high-Reynolds-number bubble rising within a thin gap. *J Fluid Mech.* 2012; 707: 444–466, doi: [10.1017/jfm.2012.289](https://doi.org/10.1017/jfm.2012.289).
5. Zhou B, Aboulhasanzadeh B, Gao P, et al. A numerical study of the phase distribution in oscillatory bubbly flows. *Int J Heat Fluid Flow.* 2018; 70: 152–159, doi: [10.1016/j.ijheatfluidflow.2018.02.004](https://doi.org/10.1016/j.ijheatfluidflow.2018.02.004).
6. Chappell MA, Payne SJ. A method for the automated detection of venous gas bubbles in humans using empirical mode decomposition. *Ann Biomed Eng.* 2005; 33(10): 1411–1421, doi: [10.1007/s10439-005-6045-8](https://doi.org/10.1007/s10439-005-6045-8), indexed in Pubmed: [16240089](https://pubmed.ncbi.nlm.nih.gov/16240089/).

7. Zueco J, López-González L. Network model to study physiological processes of hypobaric decompression sickness: New numerical results. *Acta Astronautica*. 2016; 121: 256–270, doi: [10.1016/j.actaastro.2015.12.051](https://doi.org/10.1016/j.actaastro.2015.12.051).
8. Vann RD, Butler FK, Mitchell SJ, et al. Decompression illness. *Lancet*. 2011; 377(9760): 153–164, doi: [10.1016/S0140-6736\(10\)61085-9](https://doi.org/10.1016/S0140-6736(10)61085-9), indexed in Pubmed: [21215883](https://pubmed.ncbi.nlm.nih.gov/21215883/).
9. Abishek S, King A, Narayanaswamy R. Dynamics of a Taylor bubble in steady and pulsatile co-current flow of Newtonian and shear-thinning liquids in a vertical tube. *Int J Multiphase Flow*. 2015; 74: 148–164, doi: [10.1016/j.ijmultiphaseflow.2015.04.014](https://doi.org/10.1016/j.ijmultiphaseflow.2015.04.014).
10. Alves SS, Orvalho SP, Vasconcelos J. Effect of bubble contamination on rise velocity and mass transfer. *Chem Eng Sci*. 2005; 60(1): 1–9, doi: [10.1016/j.ces.2004.07.053](https://doi.org/10.1016/j.ces.2004.07.053).
11. Song Q, Luo R, Yang X, et al. Phase distributions for upward laminar dilute bubbly flows with non-uniform bubble sizes in a vertical pipe. *Int J Multiphase Flow*. 2001; 27(2): 379–390, doi: [10.1016/s0301-9322\(00\)00025-2](https://doi.org/10.1016/s0301-9322(00)00025-2).
12. Kashinsky ON, Timkin LS, Cartellier A. Experimental study of “laminar” bubbly flows in a vertical pipe. *Exp Fluids*. 1993; 15-15(4-5): 308–314, doi: [10.1007/bf00223408](https://doi.org/10.1007/bf00223408).
13. Lopes D, Puga H, Teixeira J, et al. Blood flow simulations in patient-specific geometries of the carotid artery: A systematic review. *J Biomech*. 2020; 111: 110019, doi: [10.1016/j.jbiomech.2020.110019](https://doi.org/10.1016/j.jbiomech.2020.110019), indexed in Pubmed: [32905972](https://pubmed.ncbi.nlm.nih.gov/32905972/).
14. Sankaran S, Lesage D, Tombropoulos R, et al. Physics driven real-time blood flow simulations. *Comp Methods Applied Mech Engineer*. 2020; 364: 112963, doi: [10.1016/j.cma.2020.112963](https://doi.org/10.1016/j.cma.2020.112963).
15. Evgenidis S, Karapantsios T. Effect of bubble size on void fraction fluctuations in dispersed bubble flows. *Int J Multiphase Flow*. 2015; 75: 163–173, doi: [10.1016/j.ijmultiphaseflow.2015.05.013](https://doi.org/10.1016/j.ijmultiphaseflow.2015.05.013).
16. Evgenidis S, Karapantsios T. Gas-liquid flow of sub-millimeter bubbles at low void fractions: Experimental study of bubble size distribution and void fraction. *Int J Heat Fluid Flow*. 2018; 71: 353–365, doi: [10.1016/j.ijheatfluidflow.2018.04.011](https://doi.org/10.1016/j.ijheatfluidflow.2018.04.011).
17. Evgenidis S, Kazakis N, Karapantsios T. Bubbly flow characteristics during decompression sickness: Effect of surfactant and electrolyte on bubble size distribution. *Colloids and Surfaces A: Physicochemical and Engineering Aspects*. 2010; 365(1-3): 46–51, doi: [10.1016/j.colsurfa.2010.02.032](https://doi.org/10.1016/j.colsurfa.2010.02.032).
18. Gkotsis P, Evgenidis S, Karapantsios T. Associating void fraction signals with bubble clusters features in co-current, upward gas-liquid flow of a non-Newtonian liquid. *Int J Multiphase Flow*. 2020; 131: 103297, doi: [10.1016/j.ijmultiphaseflow.2020.103297](https://doi.org/10.1016/j.ijmultiphaseflow.2020.103297).
19. Gkotsis P, Evgenidis S, Karapantsios T. Influence of Newtonian and non-Newtonian fluid behaviour on void fraction and bubble size for a gas-liquid flow of sub-millimeter bubbles at low void fractions. *Exp Thermal Fluid Sci*. 2019; 109: 109912, doi: [10.1016/j.expthermflusci.2019.109912](https://doi.org/10.1016/j.expthermflusci.2019.109912).
20. Maurus R, Ilchenko V, Sattelmayer T. Study of the bubble characteristics and the local void fraction in subcooled flow boiling using digital imaging and analysing techniques. *Exp Thermal Fluid Sci*. 2002; 26(2-4): 147–155, doi: [10.1016/s0894-1777\(02\)00121-8](https://doi.org/10.1016/s0894-1777(02)00121-8).
21. Karapantsios TD, Evgenidis SP, Zacharias K, et al. Method for the detection and characterization of bubbles in liquids and device therefor, resp. system. European Patent Office 2016; 3005942, A1. 2016.
22. Evgenidis S, Karapantsios T. Gas-liquid flow of sub-millimeter bubbles at low void fractions: Void fraction prediction using drift-flux model. *Exp Thermal Fluid Sci*. 2018; 98: 195–205, doi: [10.1016/j.expthermflusci.2018.05.018](https://doi.org/10.1016/j.expthermflusci.2018.05.018).
23. Mohammadi MH, Sotiropoulos F, Brinkerhoff J. Eulerian-Eulerian large eddy simulation of two-phase dilute bubbly flows. *Chem Engineering Sci*. 2019; 208: 115156, doi: [10.1016/j.ces.2019.115156](https://doi.org/10.1016/j.ces.2019.115156).
24. Woodcock JP. Physical properties of blood and their influence on blood-flow measurement. *Reports on Progress in Physics*. 1975; 39(1): 65–127, doi: [10.1088/0034-4885/39/1/002](https://doi.org/10.1088/0034-4885/39/1/002).
25. King RP. Modeling and simulation of mineral processing systems. Butterworth-Heinemann, London 2000.